

Imaging and modelling from serial microscopic sections for the study of anatomy

Roman Ďurikovič *, Kazufumi Kaneda, and Hideo Yamashita

Electric Machinery Laboratory, Faculty of Engineering

Hiroshima University, Japan

Abstract

In this paper, the authors consider a system for segmenting noisy intensity images and consequent three-dimensional object reconstruction from a set of planar contours. A new semi-automatic method for extraction of contours from a sequence of cross-sectional images based on an *active contour model* (ACM) is proposed. Dynamic ACM proceeds along the sequence of cross-sections following a non-rigid motion in accordance with the organ boundary. Image texture information was employed in our model as well. Problems associated with topological reconstruction from planar contours are addressed, and several criteria promoting semi-automatic topological reconstruction are introduced. The proposed system was successfully applied to the processing of real data related to animal embryonic organs, proving that the system allows detailed modelling of irregular objects. The reconstructed models can be observed in wire-frame, solid, transparent or stereoscopic semi-transparent format. The human/computer interaction implemented in the procedure assists with problems of feature identification and object manipulation about an arbitrary axis.

Key Words: Biological structures, Three-dimensional modelling, Topological reconstruction, Feature identification

*On leave from Department of Computer Graphics and Image Processing, Faculty of Mathematics and Physics, Comenius University, Mlynská dolina, 820 13 Bratislava, Slovakia.

1 Introduction

Anatomists often undertake the task of observing the shape of a specific embryo organ contaminated by a test drug. The primary source of information during this observation procedure is a series of thin microscopic slices that render the inner organs visible. For observing the overall shape of organs, however, the slices prove rather limited, as they provide only two-dimensional information. Three-dimensional models, on the other hand, give more complete information about the shape of the structure. Reconstruction of a three-dimensional surface or volume model from two-dimensional information, therefore, is an indispensable technique for better understanding the shape and the position of an organ inside a organism.

Although three-dimensional reconstruction is widely used in computer tomography (CT) and magnetic resonance imaging (MRI), the methods do not fulfil all the needs in the field of anatomy. Anatomists seek information about the exact overall shape and try to ascertain the features that build it. The resolution in the CT and MRI methods is not high enough for the process of scanning the small structures used in embryology (around 4.5mm height in our applications). For this reason, manual sectioning followed by serial microscopy scanning is used. In anatomical fields that implement serial microscopy, an image-registration method is necessary. However, the type of hardware used in the CT and MRI methods is designed to minimise the image-registration process. Moreover, in the case of CT and MRI, voxel (volume) representation is used mainly because portion and volume are primary, while surface representation is most important in dealing with the exact shapes of anatomical structures.

1.1 Problems of 3D reconstruction and previous work

Several systems are available for reconstructing organs from serial sections (KRIETE and MAGDOWSKI, 1990; TATSUMI *et al.*, 1990). STERECON is a system (MARKO *et al.*, 1992; PERKINS *et al.*, 1993) with the capability of using stereoscopic contour tracing with a digitising pad. Another well-known package based on manual contouring was developed at Columbia University (ALLEN and LEVINTHAL, 1990).

Manual segmentation through the process of tracking organ contour lines via mouse and cursor is a time-consuming and exhausting task. Segmentation algorithms for automating this procedure are therefore desirable, but conventional image-processing methods (PITAS and VENETSANOPOULOS, 1990) using only local information are often inadequate.

1.1.1 Registration. The most obvious solution in embryology is to set common external reference marks in the paraffin block before sectioning. Four marks can be made with a laser near the object to be reconstructed. The marks on each section then determine the transformation between successive sections calculated by an automatic image-registration technique (BRON and GREMILLET, 1992). In a system developed by CARLBOM *et al.* (1994), electron microscopy images are aligned using an interactive digital blink comparator. As one image is held stationary, the user translates and rotates the other image, with the stationary and moving images shown alternately on a graphics screen. An illusion of movement is created when the images become misaligned, and the movement is minimised as the images are once again brought into alignment.

1.1.2 Segmentation. In the work of LEYMARIE (1990) the movement of living cells on a planar surface is observed by processing an animation sequence. Snakes (KASS *et al.*, 1987) are used to track the moving cell and to follow the deformations which occur as the cell moves. Carlbom *et al.* introduced the methodology of tracking boundaries of neural dendrites from serial electron microscopy (CARLBOM *et al.*, 1994). Here, the snakes are used in an interactive technique consistent with manual tracking methods. This interactive technique cannot proceed automatically from slice to slice, nor can it follow highly concave structures or those whose topology changes (branching or merging) between two successive sections.

Unfortunately, because of the complexity of microscopic images of embryo sections, the aforementioned techniques are successful only in reconstructing such higher contrast regions as the outer skin of an embryo. The techniques do not appear to be useful in inner areas. The aim of this paper, therefore, is to introduce a semi-automatic method that can track both the boundary and the topology of an organ in a section-by-section fashion.

1.1.3 Reconstruction and visualisation. The obtained traces can be displayed as a set of contours or tessellated by a triangulation technique to form a surface that can be displayed as a solid object (KANEDA *et al.*, 1987). Before the surface can be formed, it is essential to know how the contours are grouped together (the contours must be assigned to each other) in the formation of the object topology, a step called *topological reconstruction*. The simple techniques use the geometric relationship between two contours, such as the overlapping area or the distance between them. Two contours are then assigned if their distance is less than the predefined threshold (MULLER and KLINGERT, 1993). Additional information available is the topological position of contours on the slice (nesting of contours), formally represented by a *tree of nesting* (SHINAGAWA *et al.*, 1991). The root of the tree corresponds to an imaginary outer contour (image boundary) which envelops all the other contours. The successors of a vertex of the tree correspond to the contours immediately contained in the contour of that vertex.

Nevertheless, the above methods fail to reconstruct holes, often considered as a particular characteristic of branching but which connect the contours with different topological positions (different levels of nesting, see Fig. 4a) within the slice. In our work, we extend the above ideas to automatic topological reconstruction of branches and holes.

Supposing that the topology has been previously reconstructed, the next step to be solved is the problem of filling the space between planar contours. The surface is most often approximated by a set of triangles based on either a global criterion - minimum surface area (FUCHS *et al.*, 1977), maximal volume (KEPPEL, 1975) - or a local one - minimum lengths of edges (CHRISTIANSEN and SEDERBERG, 1978). For a global criterion, the problem of finding the optimal solution is reduced to a problem of finding the minimum cost cycles in a directed toroidal graph. Since global methods are unable to deal with branches, the multi-branching problem has been treated (EKOULE *et al.*, 1991; CHOI and PARK, 1994) through the introduction of an intermediate contour. Another approach is based on reducing the problem to a two-dimensional interpolation, by building as many intermediate sections as necessary for a reconstruction of the object surface (OLIVA *et al.*, 1996).

Several methods using local criteria were implemented because they can be adapted to solve the branching

problem and their calculation time is negligible compared to global methods. However, they failed in some carefully designed cases. The proposal offered in this research, therefore, is the most effective choice among the available local methods.

As an outline of our paper, first, a method of obtaining cross-sectional data along with the image-registration method is described. Then, in Section 3, an improved ACM, which is a powerful and highly automatic method for extracting contours from a set of cross-sections, is introduced. Section 4 proposes a database and automatic topological reconstruction of branches and holes. A method of filling the space between contours based on the most effective choice among implemented local triangulation methods is proposed in Section 6. Finally, the results regarding data of actual animal embryonic organs are indicated in Section 7.

2 Data Acquisition

Using manual routine processing, an embryo was sectioned with an ultramicrotome at an average thickness of between 7 and $30\mu m$. The sections were further processed and stained with hematoxylin-eosin, and then mounted on glass. Photographs of a certain magnification were taken by a camera attached to an optical microscope. The images were then stored into compact discs after they were converted into digital form with a resolution of 720×580 pixels.

To reconstruct a three-dimensional structure from the series of cross-sections, it is necessary for all sections to share a common reference coordinate system; in other words, they should be registered. The most obvious solution is to use common external reference marks set into the paraffin block before sectioning (BRON and GREMILLET, 1992). However, because some important image data used in our experiments were recorded some time ago when no reference marks were adopted, a manual image registration process was employed.

2.1 Image Registration

Sections from serial microscopy are not only translated or rotated. Often they are deformed from the heating required in preparing the tissue for display on microscopic slices. Thus, serial microscopy requires a combination of linear transformation processes in order to bring the sections into approximate alignment. We therefore adopted a combination of two methods: the landmark method (BROWN, 1992) given by a user at distinctive points; and the colour combination method, used in order to conform quickly if the results are acceptable. These methods have been employed separately in different systems with limited success. However, their combination brings together reference knowledge about sections and a quick preview of results.

A pair of associated sections was registered by using two landmarks selected on each section at a distinctive point, such as the point of a heart or the tip of a limb bud, indicated by the bright symbols X and + in Fig. 1. The vectors belonging to each cross-section and defined by the landmarks can be used to determine the translation and rotation of sections simply by aligning them. For preview purposes, initially, one of the full colour sections was tinted in green, and the other in magenta (see Figs. 1a, b). While the user manipulated the landmarks, the colour of the two sections were combined to show the overlapping regions in some shade of grey, as shown in Fig. 1c. The resultant colour differences were instructive with regard to moving the landmarks for better section registration. To provide better interactions with landmarks, a preview transformation of colour-marked images was conducted, but without using an antialiasing method. After landmarks had been selected correctly, the final transformed image was calculated by taking into account the antialiasing of image rotation (see Fig. 1d). The series of sections can be registered by repeating the registration of image pairs from top to bottom, or vice versa.

3 Contour Extraction: the ACM Model

We utilised a semi-automatic approach that extends the well-known active-contour model (KASS *et al.*, 1987) to a method that tracks both the boundary and the topology of an organ in section-by-section

Figure 1: Registration of two cross-sections of a mouse embryo. (a) (b) Static image and its successive image with selected landmarks (symbols X and +) placed at the neural tube and the anterior tip of embryo. (c) Colour merging of transformed and static images. (d) The best registration obtained.

fashion. The ACM provided significant assistance to the user in the accurate location of structure boundaries. The obtained sequence of slice images were generalised in a video where each frame had a time component. The user quickly traced a contour to roughly approximate the structure boundary for a few key-frames from a sequence. The dynamic simulation then conformed the contour to the true structure boundary and proceeded through the entire time sequence to quickly extract a sequence of profiles of the same structure.

An ACM is a deformable curve composed of abstract elastic materials minimising its potential energy. Consider an ACM $v(s, i) = (x(s, i), y(s, i))$ with a spatial parameter s and section number i defined on spaces Ω and N , respectively. Let $I(x, y)$ denote the image intensity at position (x, y) . The potential energy function of the ACM originally defined in (KASS *et al.*, 1987) consists of two components. First, the deformation energy is written as

$$E_{\text{int}}(v) = w_1(s)|v'(s)|^2 + w_2(s)|v''(s)|^2 \quad (1)$$

where the first and second derivatives of contour position v with respect to a parameter s are noted v'

and v'' . The weighting functions $w_j(s)$ control the tension and rigidity of the contour over the space Ω .

Second, the image energy computed from image intensities $I_i(x, y)$ written as

$$E_{\text{image}}(v) = G_\sigma * I_i(v) \quad (2)$$

where $G_\sigma*$ denotes the convolution with a smoothing Gaussian filter of width σ . In our previous work (ĐURIKOVIČ *et al.*, 1995), we solved four problems not addressed in the earlier work of KASS *et al.* (1987) or CARLBON *et al.* (1994). First we defined the *area energy* E_{area} giving us a contour that tends to minimise its delimited area against the length minimisation, as is found in KASS *et al.* (1987); and TERZOPOLOS and METAXAS (1991). Second, the structures in our sections are expected to generally maintain average texture properties. Therefore, the problem of poorly contrasting images is solved by a *texture representation* E_{texture} of the image against the representation of the image scale space only. Third, the profile of a structure that consists of multiple regions is found using a *contour splitting* operation. Fourth, the problem till now was to select model parameters, but with our approach, the parameters controlling the elastic process can be *set automatically* based on the initial estimation of the structure boundary. The total energy functional as proposed by ĐURIKOVIČ *et al.* (1995) is then expressed by

$$E_{\text{snake}} = \frac{1}{2} \int_{\Omega} \{E_{\text{int}}(v) + W_I E_{\text{image}}(v) + W_T E_{\text{texture}}(v) + W_A E_{\text{area}}(v)\} ds. \quad (3)$$

The weight functions W_I , W_T and W_A control the *image*, *texture* and *area* energy, respectively.

3.1 Contour Operations

The most fundamental contour operations of adding and deleting a single point are introduced. If the distance between two neighbouring points is less or greater than a given threshold, a single point from or between them is either deleted or added. For the entire contour, dividing the contour into n parts is proposed. Provided that the contour points are in a near-equilibrium configuration with respect to the internal energy, the contour is divided into two parts using the segment $v_i v_j$, if points v_i and v_j connected by vectors \mathbf{r}_{ij} , \mathbf{r}_{ji} , satisfy the following conditions:

- $|v_i - v_j| \leq d_{\text{cut}}$, where d_{cut} is a constant.

- The projections of vectors ∇E_{area} at points v_i and v_j onto the vectors \mathbf{r}_{ij} and \mathbf{r}_{ji} , respectively, have opposite directions (see Fig. 2).

Moreover, a contour is divided recursively into n parts if $n - 1$ pairs of points obeying the above conditions exist. Fig. 3 shows the significance of this property for speeding up the tracing of profiles through the sequence of slices ordered along the time axis. The initialisation of a contour position for a single (bottom) slice have been traced manually, while all other contours were obtained automatically by our ACM.

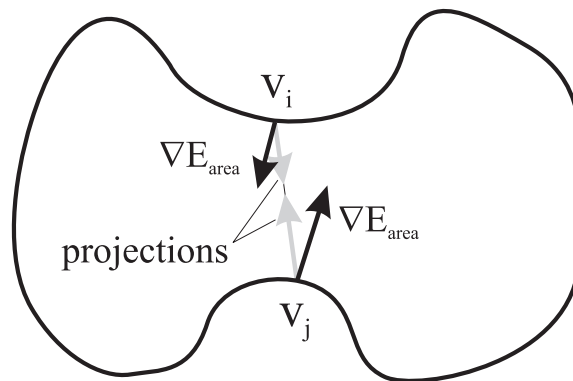


Figure 2: Conditions for cutting the ACM into two parts.

Figure 3: Automatic tracking of the structure boundary through the sequence of sections.

4 Data Structure and Topology

A hierarchical polygon data structure consists of *objects*, *sub-object surfaces*, *contours*, and *contour points*. A simple example is shown in Fig. 4a. In order to *uniquely identify* branches, each contour line is associated with a sub-object surface. The sub-object surface is part of the structure that includes neither branch nor confluence. The object consists of several sub-object surfaces, while only the connections between them create the branching (see Fig. 4b). Therefore, if a pair of contours lying in the same cross-section belongs to different sub-object surfaces, a branch must exit between the corresponding cross-sections. A hole in the surface of the object is represented as a connected branching (see Fig. 4). For example, representation of a vein passing through the hole is shown in Fig. 4b, where the inner and outer surface of the vein form two different objects ObB and ObC each consisting only of a single sub-object surface. On the other side, the object with the hole consists of five sub-object surfaces ($Sos3, \dots, Sos7$), forming two branches on the top and the bottom of the hole.

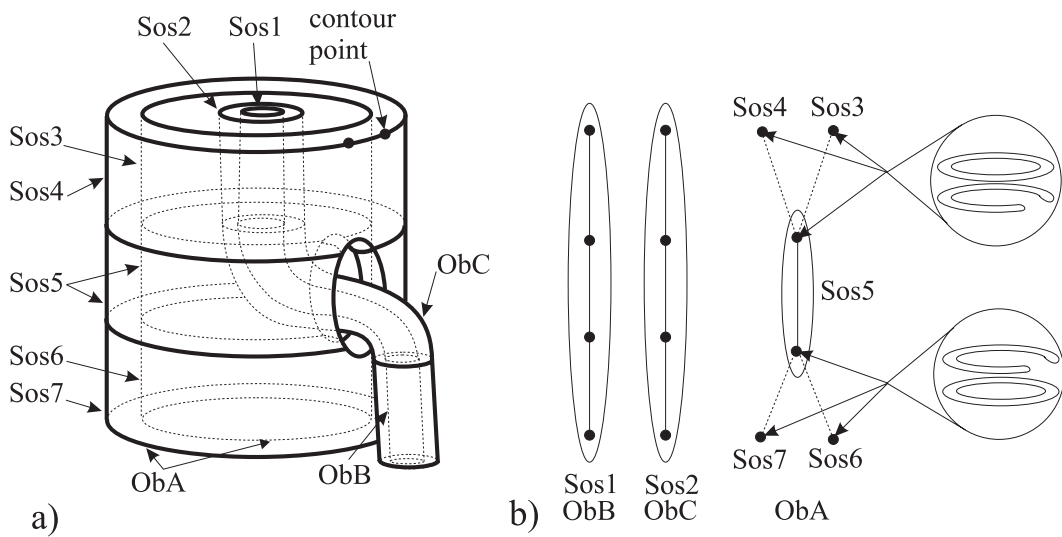


Figure 4: Hierarchical data structure and corresponding assignment graphs. a) Three objects reconstructed from four cross-sectional images: ObA consisting of sub-object surfaces $Sos3, \dots, Sos7$; ObB and ObC each consisting of a single sub-object surface $Sos1$ and $Sos2$, respectively. b) Assignment graph for the objects shown in (a), where the solid lines connect the contours of a single sub-object surface, while the broken lines denote the connection between sub-object surfaces forming the hole.

5 Automatic Topological Reconstruction

The problem of topological reconstruction is particularly difficult if there are several contours on each plane, and if it is known that the corresponding sub-object can have branches or holes. Both geometrical and topological relations between two contours are used to solve the problem of topological reconstruction. If there is a sufficient number of cross-sections for geometrical reconstruction, the proposed topological reconstruction method also works well.

5.1 Assignment Graph

Let us consider a sequence of parallel planes in space consisting of a collection of non-intersecting two-dimensional contours. The aim is to find the relations between the contours such that they will group into the sub-object surfaces, and finally, after determination of branches and holes, into the entire object. The topological reconstruction creates an output as an *assignment graph*. The vertices of the assignment graph correspond to contours, while the edges connecting the vertices form connected parts of the object, as shown in Fig. 4b. When considering the reconstruction between two cross-sections, three different types of connections are possible. These three comprise a connection between two contours (a so-called *cylindrical connection*), a connection between more than two sub-object surfaces forming an *open branch*, and a connection between the sub-object surfaces forming a hole (a *connected branch* see Fig. 4).

The proposed automatic construction of an assignment graph can be summarised in two essential steps. First, the nesting tree (SHINAGAWA *et al.*, 1991) was created for each from two successive sections. Second, pairs of contours, each from different cross-sections, were assigned to each other if they satisfied a connectivity criterion (see definition below) and occupied the same level in the nesting tree. As multiple cylindrical connections can generate branches, they were further examined based on the criteria for open branches. At this point, the cylindrical connections and open branches were determined. The connected branches (holes) were given the lowest priority, and therefore the criterion for this kind of branching was examined as the last step. The criteria used for cylindrical connections between contours and for the two

kinds of branches between sub-object surfaces are as follows.

5.2 Connectivity Criterion

Recently Muller and Klingert (MULLER and KLINGERT, 1993) proposed criteria for assigning two contours based on the average distance between contours P and Q having N_P and N_Q number of points, respectively. The contours are assumed to be planar and belong to different parallel planes. The asymmetric separation between P and Q is then expressed as

$$\delta(P, Q) = \frac{1}{\Delta_z N_P} \sum_{i=0}^{N_P} |P_i - Q_i^*|,$$

where the point $Q_i^* \in Q$ is the nearest point to $P_i \in P$ and Δ_z denotes the distance between two sections. Afterwards, they assigned two contours when $\frac{1}{2}[\delta(P, Q)]^{-1}$ is greater than a threshold value. Note that, for a particular value of i , Q_i can appear more than once in the summation. It is also worth noting that $\delta(P, Q)$ is without dimension and not metric. Unfortunately, $\delta(\cdot, \cdot)$ satisfies only one from a total of four metric conditions, namely, the non-negativity condition. The method has been used extensively and works well for partially overlapping contours. It is not sufficient, however, for contours having no common area or of very different shapes.

To solve this problem, two quasi-metrics without dimension are proposed in our approach, one measuring the separation and other measuring the relative overlap between two contours.

Definition 5.1 *Suppose two non-self-intersecting planar contours P and Q having N_P and N_Q number of points and a delimited area $A(P)$ and $A(Q)$, respectively. Their separation is defined by*

$$L(P, Q) = \frac{1}{2} (2 - [\delta(P, Q)]^{-1} - [\delta(Q, P)]^{-1}) \quad (4)$$

and their relative overlap is measured by

$$A(P, Q) = \frac{1}{2} \frac{A(Int)}{A(P)} + \frac{1}{2} \frac{A(Int)}{A(Q)}, \quad (5)$$

where $A(Int)$ is the area of intersection between contours P and Q .

Please note that for any P and Q , $L(P, Q) \in (0, 1]$ and $A(P, Q) \in [0, 1]$, respectively. Both L and A are symmetric. Separation L has a value of 0 when contours P and Q have the same shape and are close to each other. Similarly, the relative overlap A is zero for no overlap and 1 for complete overlap.

When experimenting with L and A we realised that for large contours, the criterion of relative overlap should be used primarily, while for small contours, the separation criterion is preferred. What contour is considered small is strongly dependent on image size and application area.

Definition 5.2 *A non-self-intersecting contour P lying inside an image I having area $A(P)$ and contour length l_P is considered to be small relative to the image I if*

$$S(P) = \frac{A(P)l_P}{A(I)l_I} < T_s, \quad (6)$$

where $A(I)$ is the image area and l_I is the length of the image border.

In the above definition, $S(P) \rightarrow 0$ if the delimited area by P is small, similarly $S(P) = 1$ for the largest contour, i.e. the contour identical with the image border. A threshold value $T_s \in [0, 1]$ was selected based on the application field by selecting the representative set of “small” contours and calculating the maximum of their respective value of $S(P)$. The following definition of a *connectivity criterion* accommodates the idea of selecting one of the quasi-metrics A or L based on the relative size of contours.

Definition 5.3 *The connectivity criterion for two contours P and Q is a quasi-metric defined as*

$$C(P, Q) = \begin{cases} \frac{T_s^2}{T_s^2 + S(P)S(Q)} \{L(P, Q) + \frac{S(P)S(Q)}{T_s^2} (1 - A(P, Q))\} & \text{if } S(P), S(Q) \leq T_s \\ \frac{S(P)S(Q)}{T_s^2 + S(P)S(Q)} \{ \frac{T_s^2}{S(P)S(Q)} L(P, Q) + 1 - A(P, Q) \} & \text{if } S(P), S(Q) > T_s \\ \frac{1}{2} \{L(P, Q) + 1 - A(P, Q)\} & \text{otherwise} \end{cases} \quad (7)$$

5.2.1 Cylindrical connection and open branch. All pairs of contours from consecutive sections both occupying the same level in the nesting tree and satisfying $C(P, Q) < T_c$ were assigned to each other in an assignment graph. These criteria reconstruct both the cylindrical connections and open branches.

5.2.2 Connected branch. As the criteria for assigning the connected branch (a hole), the small overlapping area and the distance between the inner contour and the one on the following or previous

section are used (see Fig. 5). In Fig. 5, the two contours A and C lying in different levels within the nesting tree are connected to a single contour B of the adjoining section. It is intuitively assumed that the shape of the hole C is similar to the open part of B . Based on this reasoning, the criteria for assigning the connected branch to the three contours A , B , and C are the measure of the largest overlapping area and the smallest distance between the *hole* and the *open part*. Additionally, contours A and B must satisfy the criteria for cylindrical connection. When there are multiple open parts in C , all parts are compared to the hole separately and the best match is selected.

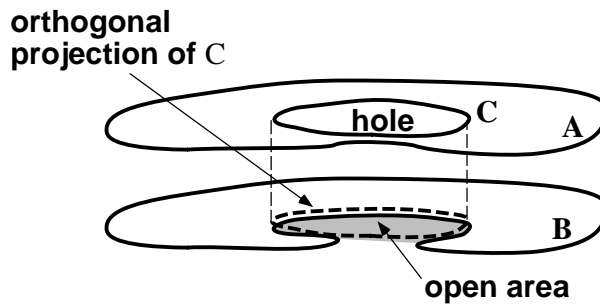


Figure 5: Measure that assigns the connected branch to the three contours based on similarity between open part and hole C .

A fully accurate reconstruction from contours is not always possible because of many valid possibilities that are unacceptable. For example, employing automatic topology reconstruction on our data sets of a mouse embryo and a frog's organs, the program correctly reconstructed 90 ~ 94% of all branches. The remaining or erroneous branches had to be corrected manually by an expert in the field.

6 Reconstruction from Contour Data

6.1 Cylindrical Connection

Let us consider the problem of filling the space between a pair of planar contours. In the proposed system, several methods using local criterion were implemented to solve the filling problem, as they can be adapted to solve the branching problem, added to their nearly negligible calculation time compared

to global methods. However, they failed in some carefully designed cases. The proposal discussed in this section is the most effective selection among available local triangulation methods. The best selection can be made based on one of the global optimum criteria, such as the minimisation of total surface area or the maximisation of volume of the reconstructed object portion. We have considered the shortest length of spans as a good choice for a selection criterion. A span is the edge of a triangle that does not belong to either planar contour.

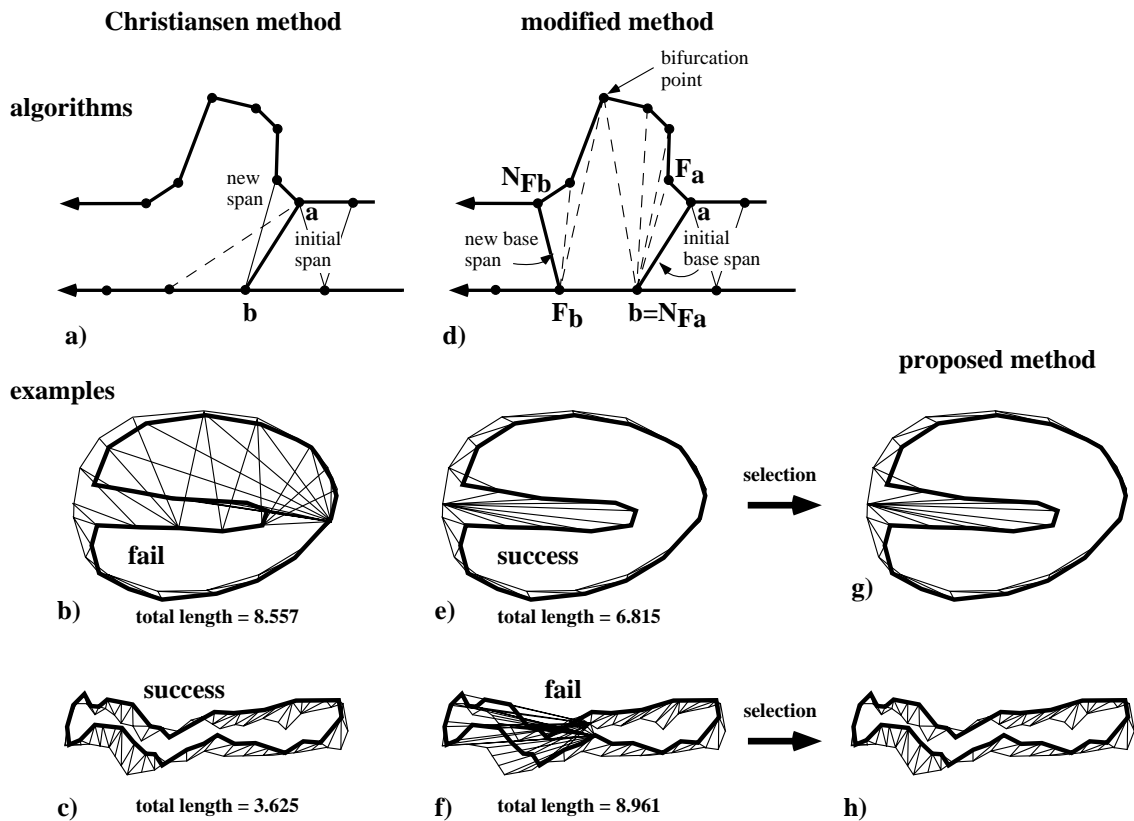


Figure 6: Generation of triangles. a) Christiansen algorithm. b) and c) Failure and success of Christiansen algorithm. d) Modified algorithm. e) and f) Success and failure of modified algorithm. g) and h) Proposed method, the selection based on the span length between Christiansen and modified method.

The filler triangular patches were generated using two local methods. The first was the Christiansen's local method (CHRISTIANSEN and SEDERBERG, 1978), which is effective for contours having similar shapes, but ineffective when the shapes vary (see Figs. 6a, 6b and 6c). The second method is a modification of the above method that was designed to reconstruct rapid changes in shape (see Figs. 6d, 6e and 6f):

1. Starting from an initial base span \mathbf{ab} , a new base span is sought.
2. For the two forward points F_a and F_b , the nearest points N_{F_a} and N_{F_b} in the neighborhood of the adjoined contour are searched (see Fig. 6d).
3. Comparing the length of spans $\overline{N_{F_a}F_a}$ and $\overline{N_{F_b}F_b}$ the shorter span is taken as the new base span.
4. The triangles between the old and new base span were then generated to minimise the total area of triangulation in this area. Next, the new base span becomes the initial base span, and the process is repeated from step 1.

Using this modification, patches such as those in Fig. 6e can be generated. The Christiansen method fails in this type of case, as shown in Fig. 6b. On the other hand, however, the modified method fails Fig. 6f when two contours are thin, even if they are of the same shape. In contrast, the Christiansen method engenders good results in this case. The combination of the above methods represents a good solution, as shown in Figs. 6g and 6h. Using more than two local methods can greatly improve results, a significant payoff for the additional time that must be invested in computation.

6.2 Open Branching

The multiple-branching problem is often treated by introducing an intermediate contour and by splitting the problem into several double-branching problems. Let the area between the multiple contour be called a channel and the inner chain of triangles filling this channel a channel polygon. The *entering* and *exiting* edge of the channel are called the bridge segments. Our particular focus is on the “optimal” determination of bridge segments as noted $\overline{B_C^2 B_D^2}$ and $\overline{B_C^1 B_D^1}$ in Fig. 7. When the bridge is found, reconstructing the channel by horizontal triangular patches within bridge segments is the simplest method.

Finding the bridge as a convex hull of the convex hulls of two contours, proposed by CHOI and PARK (1994), is often inadequate as the channel area is larger than actually necessarily. First, in this approach, the convex hull of two contours is identified, and then the convex hull of those convex hulls is calculated. There are two new segments (bridge segments) having end points in the different convex hulls of polygons.

We call this solution the *maximal bridge* because of its maximal channel area. The minimal segment between two contours determines the *minimal bridge*. An example of a maximal bridge noted by segments $\overline{M_C^2 M_D^2}$ and $\overline{M_C^1 M_D^1}$ and of a minimal bridge noted by $\overline{m_C, m_D}$ are shown in Fig. 7. The “optimal” selection of the bridge lies somewhere between the minimal and maximal bridges. The candidates for bridge segments are all segments (X_C, Y_C) having $X_C \in [M_C^2 M_C^1]$ and $Y_C \in [M_D^1 M_D^2]$. To speed up the search of bridge segments, it is sufficient to search only the set of segments filling the channel determined by the maximal bridges generated by the Christiansen method. The optimal bridge is one in which the joined contour through the bridge segments is similar to the contour in the next section. Two contours were considered similar (GONZALEZ and WINTZ, 1987) when the factor $l^2/(4\pi A)$ had a similar value for both contours, where l and A are the perimeter and area, respectively, of the surrounded region.

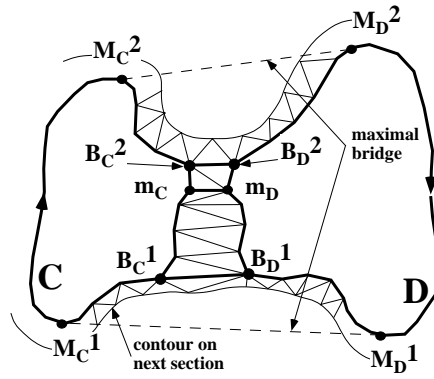


Figure 7: Finding of bridge points on a branch seen from above, $\overline{B_C^2 B_D^2}$ and $\overline{B_C^1 B_D^1}$ are automatically generated bridge segments.

7 Results

The described system for the reconstruction and analysis of optical microscope sections reduced the effort and time required to reconstruct embryological structures from a few months to only several days. As an example, a mouse embryo (4.45 mm height) was sectioned with an average section thickness of about 7 μm using an ultramicrotome. The 636 cross-sections obtained were further processed.

The proposed ACM was applied by the authors to the location of target organs within the microscopic

images and to the three-dimensional reconstruction of a mouse embryo. The new ACM offers a way to reduce the sensitivity of active contours to localised noise. The method is shown to be effective for refining estimates of an object’s shape, location and tracking any topology changes. The outlines of organs that consist of multiple branches or holes can be followed automatically from slice to slice. This phenomenon occurs within the series of cross-sections as the splitting of a contour when there is a different number of contours in two consecutive cross-sections. The result of automatic topology reconstruction is demonstrated in Fig. 8. These data contain several open and connected branches, and in the worst case 90% when measuring for each organ separately, (total in average 94%) of them were reconstructed correctly. Parameter T_s for successful topological reconstruction was calculated as the maximum value of $S(P)$ on a representative set of small contours; the result was $T_s = 0.03113$.

Another set of sections used in the study was that of frog’s cranial area. This set was selected because of complicated topology of a frog’s semicircular canals. The set consisted of 64 cross-sections with a thickness of $35\mu m$. Outlines of the semicircular canals were extracted from the sections by initialising outlines for only a single section within the entire set. With methods using only geometrical information, reconstructing the topology of the obtained contour data is extremely difficult, if not impossible. However, the proposed reconstruction method reconstructed the topology of the structure without any missassignments, as seen in Fig. 9b. Furthermore, when the triangular patches are generated, transparent and semi-transparent (KANEDA *et al.*, 1987) visualisation techniques can be applied. The transparent visualisation of the heart and blood vessels is shown in Fig. 9a.

8 Conclusions

In this paper, a system for extracting contours from multiple cross-sections and techniques for reconstruction of three-dimensional structures have been proposed. A new adaptive ACM was implemented in the proposed system. The proposed ACM can automatically follow slice to slice and can adapt its shape to highly concave structures or to those whose topology changes (branching or merging) between two successive sections. The process of topology reconstruction was improved by incorporating information

about the nesting of contours, and by the definition of quasi-metric criteria regarding when to assign two contours to each other in an assignment graph. Methods for topology reconstruction of both open and connected branching have been proposed. At the step of reconstruction, the space between two contours was filled by triangular patches resulting from the optimal solution, i.e., the most effective solution among several local optimal methods. The reconstruction of open branches can be processed more accurately using discrete optimisation of the bridge location limited to the minimal and maximal bridges.

The proposed system successfully applied to the processing of actual data related to human and animal embryonic organs proved that the system allows detailed modelling of complicated objects.

Acknowledgments

The authors wish to thank Prof. Mineo Yasuda and Prof. Akinao G. Sato for their advice and for providing the sample data of a mouse embryo. We also wish to thank Prof. Yasuo Harada for inspiration regarding the visualisation of a semicircular canal, which has complicated shapes in both planar contours and three-dimensional structures, and also for providing the cross-section images. Our thanks also to the reviewers for their helpful comments.

References

- ALLEN, B.A., and LEVINthal, C. (1990): ‘CARTOS II semi-automated nerve tracing: three-dimensional reconstruction from serial section micrographs’, *Computerized Medical Imaging and Graphics*, **14**, pp. 319–329
- BRON, C., and GREMILLET, P. (1992): ‘3-D reconstructions by image-processing of serial sections in electron microscopy’, *in* KRIETE, A. (Ed.): ‘Visualization in biomedical microscopies: 3-D imaging and

Figure 8: Reconstructed topology of 54 objects of mouse embryo. Grey structure is a neural tube, light brown structure in the middle is a heart with blood vessels coloured dark brown. Stomach is the structure behind the heart coloured magenta.

Figure 9: Transparent visualisation of reconstructed structures. a) Mouse embryo's heart and blood vessels. b) Complicated topology of left and right frog semicircular canals.

computer applications' (VCH Publishers, Weinheim), pp. 75–105

BROWN, J.P. (1992): 'A survey of image registration techniques', *Computing Surveys*, **24**, pp. 325–376

CHOI, Y.K., and PARK, K.H. (1994): 'A heuristic triangulation algorithm for multiple planar contours using an extended double branching procedure', *The Visual Computer*, **10**, pp. 372–387

CHRISTIANSEN, H.N., and SEDERBERG, T.W. (1978): 'Conversion of complex contour line definitions into polygonal element mosaics', *Computer Graphics (SIGGRAPH '78 Proceedings)*, pp. 187–192

CARLBOM, I., TERZOPOULOS, D., and HARRIS, K.M. (1994): 'Computer-assisted registration, segmentation, and 3D reconstruction from images of neural tissue sections', *IEEE Transaction of Medical Imaging*, **13**, pp. 351–362

ĐURIKOVIČ, R., KANEDA, K., and YAMASHITA, H. (1995): 'Dynamic contour: A texture approach and contour operations', *The Visual Computer*, **11**, pp. 277-289

FUCHS, H., KEDEN, Z.M., and USELTON, S.P. (1977): 'Optimal surface reconstruction from planar contours', *Communication ACM*, **20**, pp. 693–702

GONZALEZ, R.C., and WINTZ, P. (1987): 'Digital image processing', 2 edition, (Addison-Wesley Publishing Company, Reading, Massachusetts)

KANEDA, K., HARADA, K., NAKAMAE, E., YASUDA, M., and SATO, A.G. (1987): 'Reconstruction and semi-transparent display method for observing inner structure of an object consisting of multiple surfaces', *The Visual Computer*, **3**, pp. 137–144

KASS, M., WITKIN, A., and TERZOPOULOS, D. (1987): 'Snakes: Active contour models. *International Journal of Computer Vision*, **4**, pp. 321–331

KEPPEL, E. (1975): 'Approximating complex surfaces by triangulation of contour lines', *IBM J. Res. Dev.*, **19**, pp. 2-11

KRIETE, A., and MAGDOWSKI, G. (1990): 'Computerized three-dimensional image processing of serial

sections in electron microscopy', *Ultramicroscopy*, **32**, pp. 48–54

LEYMARIE, F. (1990): 'Tracking and describing deformable objects using active contour models', Master's thesis, (McGill University, Montreal, Canada)

MARKO, M., and LEITH, A. (1992): 'Contour-based 3-D surface reconstruction using stereoscopic contouring and digitized images' in KRIETE, A. (Ed.): 'Visualization in biomedical microscopies: 3-D imaging and computer applications' (VCH Publishers, Weinheim), pp. 45–73

MULLER, H., and KLINGERT, A. (1993): 'Surface interpolation from cross sections' in NIELSON, G.M., HAGEN, H., and MULLER, H. (Eds.): 'Focus on scientific visualization' (Springer-Verlag, Berlin Heidelberg), pp. 139–189

OLIVA, J.M., PERRIN, M., and COQUILLART, S. (1996): '3D reconstruction of complex polyhedral shapes from contours using a simplified generalized Voronoi diagram' in ROSSIGNAC, J., and SILLION, F. (Eds.): 'EUROGRAPHICS '96' (Blackwell Publishers,), pp. 397–408

PITAS, I., and VENETSANOPOULOS, A.N. (1990): 'Nonlinear digital filters: principles and applications' (Kluwer Academic, Boston Dordrecht London), pp. 276–344

PERKINS, W.J., HASHMI, S., and JORDAN, M. (1993): 'Three-dimensional computer modelling system for the study of biological structures', *Med. & Biol. Eng. & Comput.*, **31**, pp. 557–561

SHINAGAWA, Y., KUNII, T.L., and KERGOSIEN, Y.L. (1991): 'Surface coding based on Morse theory', *IEEE Computer Graphics and Applications*, **11**, pp. 66–78

TATSUMI, H., TAKAOKI, E., OMURA, K., and FUJITA, H. (1990): 'A new method for three-dimensional reconstruction from serial sections by computer graphics using meta-balls: reconstruction of the hepatoskeletal system formed by Ito cells in the cod liver', *Comput. Biomed. Res.*, **23**, pp. 37–45

TERZOPOULOS, D., and WATERS, K. (1990): 'Analysis of facial images using physical and anatomical models', *Proceedings of 3rd International Conference on Computer Vision*, pp. 727–732

List of Figures

1	Registration of two cross-sections of a mouse embryo. (a) (b) Static image and its successive image with selected landmarks (symbols X and +) placed at the neural tube and the anterior tip of embryo. (c) Colour merging of transformed and static images. (d) The best registration obtained.	7
2	Conditions for cutting the ACM into two parts.	9
3	Automatic tracking of the structure boundary through the sequence of sections.	9
4	Hierarchical data structure and corresponding assignment graphs. a) Three objects reconstructed from four cross-sectional images: <i>ObA</i> consisting of sub-object surfaces <i>Sos3</i> , . . . , <i>Sos7</i> ; <i>ObB</i> and <i>ObC</i> each consisting of a single sub-object surface <i>Sos1</i> and <i>Sos2</i> , respectively. b) Assignment graph for the objects shown in (a), where the solid lines connect the contours of a single sub-object surface, while the broken lines denote the connection between sub-object surfaces forming the hole.	10
5	Measure that assigns the connected branch to the three contours based on similarity between open part and hole <i>C</i>	14
6	Generation of triangles. a) Christiansen algorithm. b) and c) Failure and success of Christiansen algorithm. d) Modified algorithm. e) and f) Success and failure of modified algorithm. g) and h) Proposed method, the selection based on the span length between Christiansen and modified method.	15
7	Finding of bridge points on a branch seen from above, $\overline{B_C^2 B_D^2}$ and $\overline{B_C^1 B_D^1}$ are automatically generated bridge segments.	17
8	Reconstructed topology of 54 objects of mouse embryo. Grey structure is a neural tube, light brown structure in the middle is a heart with blood vessels coloured dark brown. Stomach is the structure behind the heart coloured magenta.	20

9 Transparent visualisation of reconstructed structures. a) Mouse embryo's heart and blood vessels. b) Complicated topology of left and right frog semicircular canals. 20